

Article

Synthesis and preliminary studies of a novel negative allosteric modulator [C]QCA for imaging of metabotropic glutamate receptor 2

Xiaofei Zhang, Katsushi Kumata, Tomoteru Yamasaki, Ran Cheng, Akiko Hatori, Longle Ma, Yiding Zhang, Lin Xie, Lu Wang, Hye Jin Kang, Douglas J. Sheffler, Nicholas D.P. Cosford, Ming-Rong Zhang, and Steven H Liang

ACS Chem. Neurosci., **Just Accepted Manuscript** • DOI: 10.1021/acscchemneuro.7b00098 • Publication Date (Web): 31 May 2017

Downloaded from <http://pubs.acs.org> on June 12, 2017

Just Accepted

"Just Accepted" manuscripts have been peer-reviewed and accepted for publication. They are posted online prior to technical editing, formatting for publication and author proofing. The American Chemical Society provides "Just Accepted" as a free service to the research community to expedite the dissemination of scientific material as soon as possible after acceptance. "Just Accepted" manuscripts appear in full in PDF format accompanied by an HTML abstract. "Just Accepted" manuscripts have been fully peer reviewed, but should not be considered the official version of record. They are accessible to all readers and citable by the Digital Object Identifier (DOI®). "Just Accepted" is an optional service offered to authors. Therefore, the "Just Accepted" Web site may not include all articles that will be published in the journal. After a manuscript is technically edited and formatted, it will be removed from the "Just Accepted" Web site and published as an ASAP article. Note that technical editing may introduce minor changes to the manuscript text and/or graphics which could affect content, and all legal disclaimers and ethical guidelines that apply to the journal pertain. ACS cannot be held responsible for errors or consequences arising from the use of information contained in these "Just Accepted" manuscripts.

Synthesis and preliminary studies of a novel negative allosteric modulator [¹¹C]QCA for imaging of metabotropic glutamate receptor 2

Xiaofei Zhang,^{†,‡,§} Katsushi Kumata,^{‡,§} Tomoteru Yamasaki,[‡] Ran Cheng,[†] Akiko Hatori,[‡]
Longle Ma,[†] Yiding Zhang,[‡] Lin Xie,[‡] Lu Wang,[†] Hye Jin Kang,[⊥] Douglas J. Sheffler,[§]
Nicholas D. P. Cosford,[§] Ming-Rong Zhang^{*,‡} and Steven H. Liang^{*,†}

[†] Nuclear Medicine and Molecular Imaging, Massachusetts General Hospital & Department of Radiology, Harvard Medical School, Boston, MA, 02114, USA.

[‡]State Key Laboratory and Institute of Elemento-Organic Chemistry, Collaborative Innovation Center of Chemical Science and Engineering, Nankai University, Tianjin 300071, China

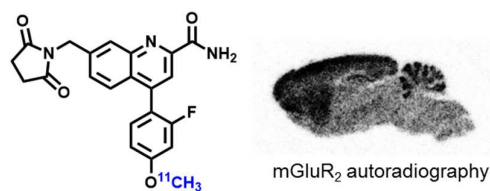
[‡]Department of Radiopharmaceutics Development, National Institute of Radiological Sciences, National Institutes for Quantum and Radiological Science and Technology, Chiba, 263-8555, Japan.

[⊥]Department of Pharmacology & National Institute of Mental Health Psychoactive Drug Screening Program, University of North Carolina at Chapel Hill, North Carolina, 27515, USA.

[§]Cell Death and Survival Networks Program and Conrad Prebys Center for Chemical Genomics, Sanford-Burnham Medical Research Institute, La Jolla, CA, 92037, USA.

[#]These authors contribute equally to this work.

Abstract: Metabotropic glutamate 2 receptors (mGlu₂) are involved in the pathogenesis of several CNS disorders and neurodegenerative diseases. Pharmacological modulation of this target represents a potential disease-modifying approach for the treatment of substance abuse, depression, schizophrenia and dementias. While quantification of mGlu₂ receptors in the living brain by positron emission tomography (PET) would help us better understand signaling pathways relevant to these conditions, few successful examples have been demonstrated to image mGlu₂ in vivo and a suitable PET tracer is yet to be identified. Herein we report the design and synthesis of a radiolabeled negative allosteric modulator (NAM) for mGlu₂ PET tracer development based on a quinoline 2-carboxamide scaffold. The most promising candidate, 7-((2,5-dioxopyrrolidin-1-yl)methyl)-4-(2-fluoro-4-[¹¹C]methoxyphenyl) quinoline-2-carboxamide ([¹¹C]QCA) was prepared in 13% radiochemical yield (non-decay corrected at the end of synthesis) with >99% radiochemical purity and >74 GBq/μmol (2 Ci/μmol) specific activity. While the tracer showed limited brain uptake (0.3 SUV), probably attributable to effects on PgP/Bcrp efflux pump, in vitro autoradiography studies demonstrated heterogeneous brain distribution and specific binding. Thus, [¹¹C]QCA is a chemical probe that provides the basis for the development of a new generation mGlu₂ PET tracers.



Keywords: positron emission tomography, metabotropic glutamate receptor 2, mGlu₂, ¹¹C, negative allosteric modulator

INTRODUCTION

Glutamate is the most abundant endogenous excitatory neurotransmitter and glutamate receptors (Glu) play a pivotal role in modulating a wide scope of neurological functions in the central nervous system (CNS).¹⁻⁶ Glutamatergic signaling is primarily mediated via two distinct groups, namely ionotropic receptors (iGlu) and the G protein-coupled metabotropic receptors (mGlu). Based on different sequence homology, anatomical distribution and pharmacology, the mGlu are typically divided into three subcategories. Group I mGlu (mGlu₁ and mGlu₅), coupled to G_q/G₁₁ proteins, mobilize calcium from intracellular stores upon activation and increase protein kinase C activity. Group II (mGlu₂ and mGlu₃) and Group III (mGlu₄, mGlu₆, mGlu₇ and mGlu₈) mGlu, coupled to G_{i/o} proteins, downregulate cAMP formation through inhibition of adenylyl cyclase.⁷ In particular, mGlu₂ receptors negatively regulate endogenous glutamate release and consequently may be involved in the protection of neurons against excitotoxicity. The receptors are predominantly localized on presynaptic membranes although they are also found in peripheral regions of the synapse.^{8,9} Moderate-to-high expression of mGlu₂ can be found in many brain regions, including the cerebral cortex, cerebellum, amygdala and hippocampus.¹⁰⁻¹⁴ It has been reported that mGlu₂ is involved in the pathogenesis of numerous brain dysfunctions, including psychiatric disorders and neurodegenerative diseases.^{7,15-19} Therefore pharmacological modulation of mGlu₂ represents a promising therapeutic approach for the treatment of several CNS diseases,²⁰ including drug dependence,²¹⁻²³ chronic pain,²⁴ anxiety,¹⁷ depression,^{25,26} schizophrenia,²⁷ Parkinson's disease^{28,29} and Alzheimer's disease.³⁰ Initial drug discovery efforts focused on non-selective mGlu_{2/3} agonists and antagonists that bind to the mGlu orthosteric binding site (evolutionarily conserved glutamate binding site);³¹ however, in recent years there has been a shift towards allosteric modulation strategies (consisting of positive and negative allosteric modulators; abbreviated as PAM and NAM, respectively) that offer the potential for improved selectivity for mGlu₂ or mGlu₃.^{32,33} While a wide range of highly selective mGlu₂ PAMs have been discovered and recently reviewed,^{33,34} the development of selective mGlu₂ NAMs has remained in its nascent stage with only one report based on a dihydroquinoline 2-carboxamide scaffold in the primary literature.³⁵

Positron emission tomography (PET) is a non-invasive imaging technology that is capable of quantifying biochemical processes in vivo,³⁶⁻³⁹ which would enable investigations of mGlu₂ based glutamatergic signaling under normal and disease conditions, and assessment of distribution and testing target engagement and dose occupancy of mGlu₂ drug candidates for clinical trials. Unlike several mGlu₁ or mGlu₅-targeting PET radiotracers in human use,⁴⁰⁻⁴⁵ there is an unmet need for probing mGlu₂ in clinical research and drug development towards this important receptor subtype in the glutamatergic pathway. As shown in **Figure 1**, there are continuous research efforts in the development of mGlu₂ PET tracers,⁴⁰⁻⁴³ including [¹¹C]CMGDE (**1**),^{46,47} [¹¹C]JNJ-42491293 (**2**),^{48,49} [¹⁸F]FE-JNJ42491293 (**3**),⁵⁰ [¹¹C]CMD C (**4**)⁵¹ and two tracers (¹⁸F-compound **5** and ¹¹C-compound **6**) in the patent literature.^{52,53} Among these studies [¹¹C]CMGDE (**1**), the first mGlu₂ radiotracer based on a prodrug of an antagonist LY341495, provided a foundation for the further development of a specific mGlu₂

tracer.⁴⁷ On the other hand [¹¹C]CMDC (**4**), a derivative of JNJ-40068782,⁵⁴ was not further pursued due to limited brain penetration (peak brain uptake *ca.* 0.6 SUV).⁵¹ Preliminary evaluation in PET imaging studies for compounds **3**, **5**, **6** are not yet disclosed for the development of mGlu₂ tracers.^{52,53} Only two PET tracers, namely [¹¹C]JNJ-42491293 (**2**) and a ¹¹C-compound from Merck, have been advanced to first-in-human studies. [¹¹C]JNJ-42491293 (**2**) was discontinued for mGlu₂ imaging due to unexpected off-target binding in vivo during clinical trials^{55,56} and only limited preliminary data on the Merck compound (no structural information) were reported in abstracts.^{57,58} These mGlu₂ imaging efforts combined with pharmaceutical development and the potential of mGlu₂-modulating pharmacotherapy provide a strong impetus to advance PET tracer development for this target.

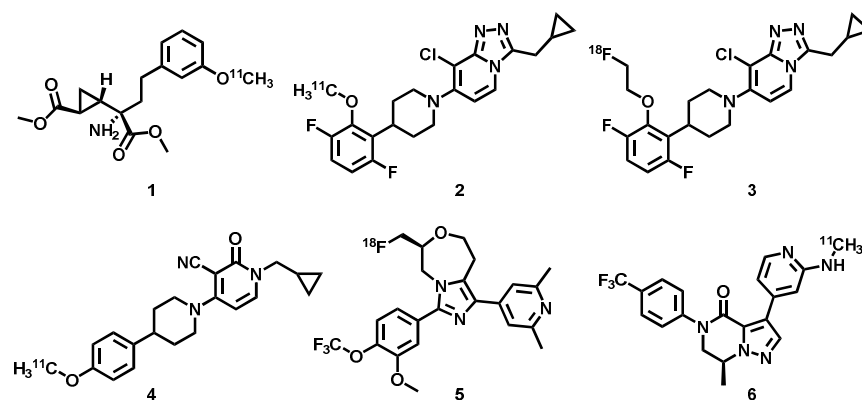


Figure 1. PET tracers targeting mGlu₂. While the majority of compounds in this figure have no selectivity data available in the primary literature, compound **2** showed mGlu₂ selectivity greater than 350 fold over the other mGlu receptors.⁴⁹

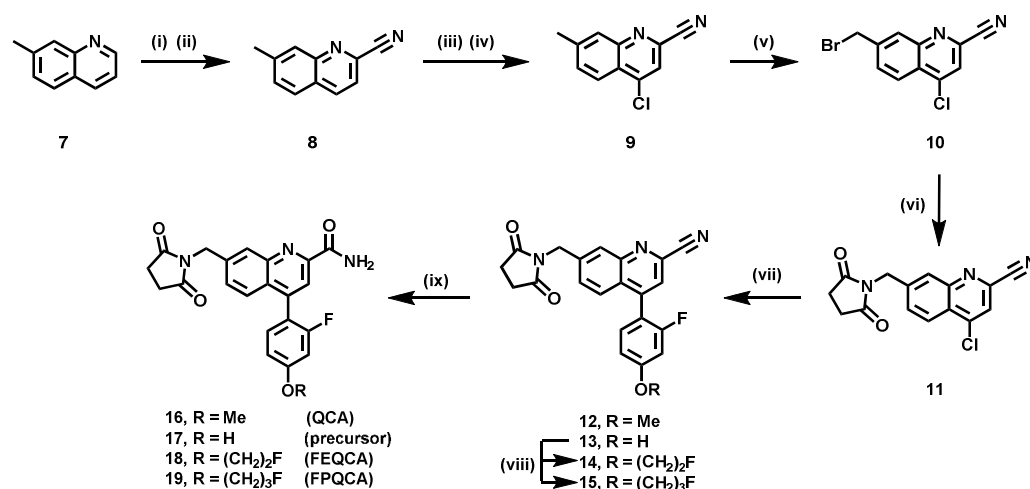
Herein we describe the synthesis of a small array of potent and selective mGlu₂ NAMs that are amenable for radiolabeling and their preliminary evaluation in rodents by PET. In vitro autoradiography studies confirm the specific binding of these new NAMs bearing a quinoline 2-carboxamide moiety, which provides an excellent starting point for future mGlu₂ PET tracer design.

RESULTS AND DISCUSSION

Chemistry. We designed a focused library of small molecule based on a series of NAMs disclosed in the patent literature,⁵⁹ with the goal to develop a selective mGlu₂ PET tracer amenable to radiolabeling with either ¹¹C or ¹⁸F. In particular, the succinimidyl compound **16** was selected in our proof-of-concept studies because of reported low EC₅₀ value (8 nM), reasonable cLogP value (2.95) and amenability for ¹¹C-labeling from its corresponding phenolic precursor. Thus a set of quinolone 2-carboxamides and their labeling precursors were synthesized according to our synthetic strategy (see detailed retrosynthetic analysis in **Scheme S1** of Supporting Information, SI). As summarized in **Scheme 1**, oxidation of 7-methylquinoline (**7**) with *m*CPBA followed by cyanide addition provided quinoline-2-carbonitrile **8** in 74% yield over two steps, which was converted to chloroquinoline **9** after *m*CPBA oxidation and POCl₃ chlorination (60% yield). Site-specific

bromination at the benzyl position of chloroquinoline **9** followed by succinimide substitution gave key intermediate **11** in 80% yield. Several parallel syntheses were carried out to introduce aryl groups at the ipso position of the chloride via palladium catalyzed Suzuki cross-coupling reactions. The coupling reaction with (2-fluoro-4-methoxyphenyl)boronic acid gave quinoline nitrile **12**, which was hydrolyzed in basic H_2O_2 solution to afford the final standard

7-((2,5-dioxopyrrolidin-1-yl)methyl)-4-(2-fluoro-4-methoxyphenyl)quinoline-2-carboxamide (QCA; **16**) in 55% yield over 2 steps. The cross coupling procedure was also applied to obtain phenol **17** (51% yield), fluoroethyl (FEPAD (**18**), 60% yield) and fluoropropyl derivatives (FPPAD (**19**), 53% yield). In brief, the synthesis of QCA (**16**), its precursor **17** and fluorinated derivatives (**18-19**) were achieved in eight to nine steps with overall yields of 6% - 10%.



Scheme 1. Synthesis of quinoline 2-carboxamide analogs. (i) *m*CPBA, DCM, 1h; (ii) TMSCN, dimethylcarbamic chloride, DCM, 12 h, 74% for two steps; (iii) *m*CPBA, DCM, 40 °C, 4 h; (iv) POCl_3 , DMF, CHCl_3 , 70°C, 6 h, 64% yield for two steps; (v) NBS, Benzoyl peroxide, CCl_4 , 85°C, 4 h, 60% yield; (vi) succinimide, Cs_2CO_3 , DMF, 30 min, 80% yield; (vii) arylboronic acid, $\text{Pd}(\text{PPh}_3)_4$, Na_2CO_3 , 1,4-dioxane, H_2O , 100°C; (viii) Cs_2CO_3 , DMF, 12 h, $\text{IC}_2\text{H}_4\text{F}$ for **14**, 45% yield over 2 steps from **11**; $\text{IC}_3\text{H}_6\text{F}$ for **15**, 53% yield over 2 steps from **11**; (ix) sodium percarbonate, 55% yield for QCA (**16**) over 2 steps from **11**, 51% yield for precursor **17** over 2 steps from **11**, 60% yield for FEQCA (**18**), and 53% yield for FPQCA (**19**).

Pharmacology and physicochemical properties. QCA and its two fluorinated derivatives (FEQCA and FPQCA) were subsequently screened for their *in vitro* activity towards mGlu_2 and mGlu_3 , and the results are shown in **Figure 2**. A thallium flux assay in human embryonic kidney 293 (HEK) cells expressing heteromeric G-protein coupled inwardly rectifying potassium (GIRK) channels⁶⁰ and human mGlu_2 or mGlu_3 , was utilized to determine potency, efficacy and selectivity. The concentration-response relationship that antagonizes the effect of an EC_{80} concentration of glutamate was determined for each candidate. Potency is expressed as the IC_{50} for inhibition of the glutamate EC_{80} response. All three candidates showed NAM activity (IC_{50} values 45 ± 5 nM for QCA, 130 ± 10 nM for

FEQCA, and 1080 ± 1300 nM for FPQCA) at human mGlu₂ and excellent selectivity for mGlu₂ over mGlu₃. We utilized MNI-137, a mGlu_{2/3} NAM, as a positive control in our GIRK assay,⁶¹ and found no evidence of mGlu₃ potencies up to the highest concentration of 30 μ M. In addition, QCA was inactive towards other mGlu receptors at the test concentration of 30 μ M, and showed no significant interaction with major CNS targets, which was conducted via GPCRome assays⁶² developed by the NIH PDSP program. (see excel data sheet in the associate content).

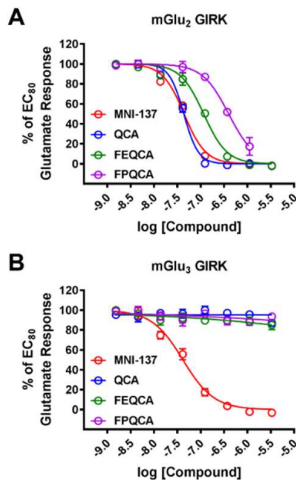


Figure 2. In vitro evaluation of the potencies of QCA, FEQCA, FPQCA, and the control mGlu_{2/3} NAM MNI-137 in mGlu₂ GIRK (A) or mGlu₃ GIRK (B) functional assays.

We next evaluated whether QCA inhibits mGlu₂ by a competitive or noncompetitive mechanism of action in functional studies by performing a Schild analysis.⁶³ For these studies, the concentration-response relationships of glutamate-induced increases in thallium flux were evaluated for both mGlu₂ and mGlu₃ in the absence or presence (30 μ M, 10 μ M, 3333 nM, 1111 nM, 370 nM, 123 nM, or 41 nM) of QCA (**Figure 3**). QCA dose-dependently right-shifted the concentration-response of glutamate toward mGlu₂ (**Figure 3A**) and decreased the maximal glutamate response, consistent with a noncompetitive mode of action. Alternatively, consistent with the previous in vitro studies (Figure 2B), QCA had no effect on either the glutamate potency or glutamate maximal response toward mGlu₃ (**Figure 3B**), which also serves as an additional control demonstrating the mGlu₂ selectivity of QCA.

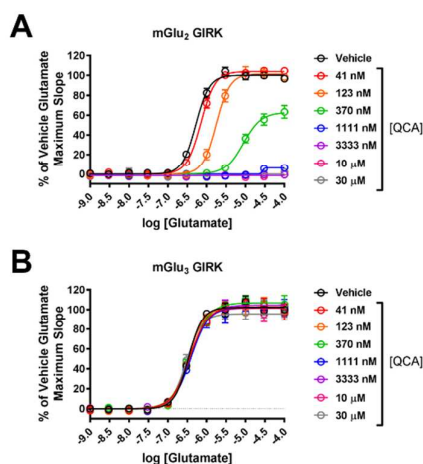


Figure 3. QCA noncompetitively right-shifts the glutamate concentration-response for mGlu₂ and decreases the maximal glutamate response (A) but has no effect on the glutamate concentration-response for mGlu₃ (B).

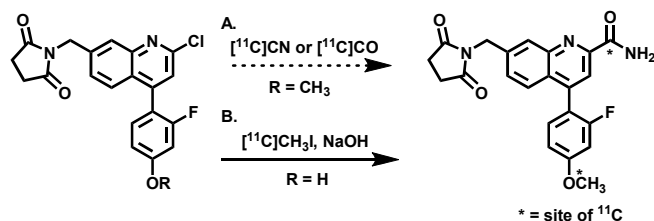
Lipophilicity of candidate compounds can be used as a predictive parameter for assessing blood-brain barrier permeability, with preferred range of 1.0-3.5.⁶⁴⁻⁶⁶ The cLogP values of compounds QCA (**16**), FEQCA (**18**) and FPQCA (**19**) were predicted to be 2.95, 3.44 and 3.69, respectively, using Pallas 3.0 prediction software (**Table 1**). Using liquid-liquid partition between *n*-octanol and water ("shake flask method"),⁶⁷ the LogP values for QCA, FEQCA, and FPQCA were 1.27 ± 0.29 , 1.75 ± 0.14 and 1.99 ± 0.12 , respectively. Since *in vitro* assessments of pH stability, plasma and microsomal stability are important to the initial selection of candidate compounds,⁶⁸ we carried out preliminary experiments to determine these parameters. We first evaluated the stability of the compounds under physiological conditions (pH = 5.0-9.4). All three compounds showed excellent stability at pH 5 and diminished stability at pH 7.4 and 9.4 at 37°C, which may be attributed to hydrolysis of succinimidyl group at higher pH. In addition, QCA and its fluorinated derivatives showed reasonable plasma and microsomal stability. Based on the functional assay results (*cf.* Figs. 2 & 3) and physicochemical properties (*cf.* Table 1), QCA (**16**) exhibited the lowest EC₅₀ value among all derivatives and reasonable lipophilicity and plasma/microsomal stability, which warrants further radiolabeling and subsequent evaluation by *in vivo* PET imaging and *ex vivo* biodistribution studies.

Entry	lipophilicity ^a		pH stability ^b			plasma stability ^c	microsomal stability ^d
	cLogP	LogP	5.0	7.4	9.4		
16	2.95	1.27	97.9%	50.9%	46.7%	22.5%	64.4%
18	3.44	1.75	98.5%	53.6%	59.0%	46.7%	70.1%
19	3.69	1.99	91.5%	72.5%	76.3%	87.5%	64.6%

Table 1. Physicochemical properties of QCA (**16**), FEQCA (**18**) and FPQCA (**19**).

^alipophilicity is calculated and measured by Pallas 3.0 software and the shake flask method, respectively. ^{b-d}percent (average, *n* ≥ 3) remaining of the parent molecule after incubation at 37 °C for 60 min. ^cdiltiazem and ^dverapamil as positive controls, respectively.

Radiochemistry. As shown in **Scheme 2**, there are three possible labeling strategies for QCA (**16**), namely (1) ^{11}C -cyanation followed by H_2O_2 hydrolysis from 2-chloroquinoline precursor; (2) ^{11}C -carbonylation via $[^{11}\text{C}]\text{CO}$ followed by aminolysis from 2-chloroquinoline precursor and (3) ^{11}C -methylation from the phenolic precursor **17**. Although the first two approaches may entail a general and unified strategy for the formation of ^{11}C -carbonyl labeled quinoline carboxamides, as proof of concept, we chose the most convenient phenolic site for QCA labeling. The radiosynthesis of $[^{11}\text{C}]\text{QCA}$ was performed by the reaction of the phenolic precursor **17** (0.5 mg) with $[^{11}\text{C}]\text{CH}_3\text{I}$ in the presence of NaOH (1.25 μmol) in DMF (300 μL). The reaction was carried out at 80 $^\circ\text{C}$ for 5 min, followed by purification using semi-preparative HPLC. Specifically, $[^{11}\text{C}]\text{QCA}$ was obtained from the reaction between its phenolic precursor and $[^{11}\text{C}]\text{CH}_3\text{I}$. The radiochemical yield was $13 \pm 4\%$ non-decay corrected ($n = 3$), calculated from starting $[^{11}\text{C}]\text{CO}_2$. The $[^{11}\text{C}]\text{QCA}$ was then reformulated in a saline solution containing 100 μL of 25% ascorbic acid in sterile water and 100 μL of 20% Tween[®] 80 in ethanol at the end of synthesis (see details in Methods). The radiochemical and chemical purity were greater than 99% and specific activity was greater than 74 GBq/ μmol (2 Ci/ μmol). The overall synthesis time was *ca.* 30 min and no radiolysis was observed up to 90 min.



Scheme 2. Radiosynthesis of $[^{11}\text{C}]\text{QCA}$ (A) potential labeling methods; (B) $^{11}\text{CH}_3\text{I}$ labeling method.

Whole body biodistribution studies in mice. The uptake, distribution and clearance of $[^{11}\text{C}]\text{QCA}$ ($[^{11}\text{C}]\text{16}$) were studied in mice at five time points (1, 5, 15, 30 and 60 min) post tracer injection. The results are expressed as the percentage of the injected dose per gram of wet tissue (%ID/g) in **Figure 4** and **Table S1** (SI) and standardized uptake value (SUV) in **Figure S1** and **Table S2** (SI). High uptake ($>3\%$ ID/g) was observed in the heart, lungs, liver, pancreas, kidneys and small intestine at 1 min post injection of $[^{11}\text{C}]\text{QCA}$. After the initial phase the radioactivity levels in most tissues decreased rapidly, while the signals in the liver and small intestine continually increased until 30 min and then decreased slowly. The radioactivity was efficiently cleared from blood (1 min/60 min ratio of 2.4) and high radioactivity in the liver, kidneys and small intestine indicated urinary and hepatobiliary excretion, as well as a possible intestinal reuptake pathway. The distribution of $[^{11}\text{C}]\text{QCA}$ in the peripheral organs was similar to prior reports with other compounds,^{51,56,69,70} in which rapid clearance of radioactivity from heart, lungs, spleen and muscle was observed. Limited brain uptake (peak value 0.42% ID/g at 1 min post injection) was observed, and thus the regional brain distribution was further studied by in vitro autoradiography.

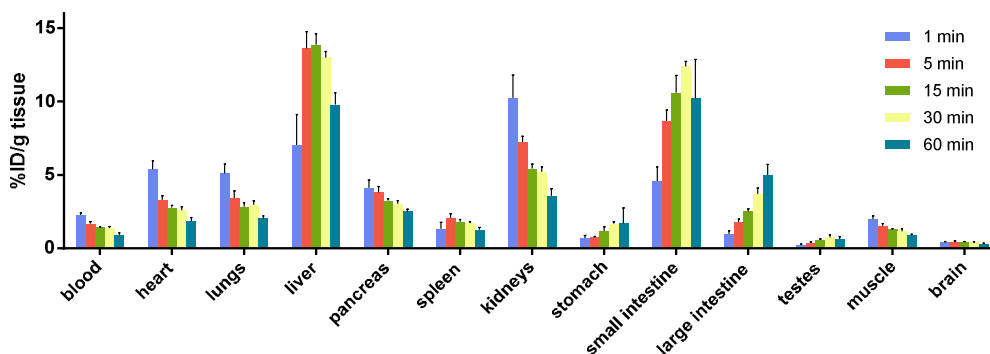


Figure 4. Ex vivo biodistribution in mice at five different time points (1, 5, 15, 30 and 60 min) post [^{11}C]QCA injection. Data are expressed as %ID/g.

In vitro Autoradiography. The binding specificity of [^{11}C]QCA to mGlu $_2$ was confirmed by in vitro autoradiography. Representative in vitro autograms of [^{11}C]QCA on sagittal sections of rat brains are shown in **Figure 5A**. In the baseline study, the distribution of bound radioactivity was heterogeneous with signal levels from high to low in the order of cerebral cortex, striatum, hippocampus, cerebellum and pons/medulla (**Figure 5B**). These autographic results are in agreement with both the previously published distribution of mGlu $_2$ in rat brain,^{10,12} and with other autoradiography studies with the mGlu $_2$ radioligands [^{11}C]CMDC,⁵¹ [^3H]JNJ-40068782,⁵⁴ [^3H]LY341495⁷¹ and [^3H]LY459477.¹⁴ As shown in **Figure 5C**, quantitative analysis of radioactivity binding in the mGlu $_2$ -rich regions (cerebral cortex, striatum, hippocampus and cerebellum) with unlabeled QCA (1 μM) and a NAM MNI-137⁶¹ (1 μM) showed ca. 50-60% reduced binding compared with that of baseline. We also observed marginal reductions (ca. 10-20%) of radioactivity binding when a mGlu $_2$ PAM LY487379⁷² was used for blocking study, which may indicate a possible shared, yet at a low level, binding site between positive and negative allosteric modulators.^{73,74} These results indicate that [^{11}C]QCA has a moderate-to-high level of in vitro specific binding to mGlu $_2$ and the binding mechanism is consistent with that of a negative allosteric modulator.

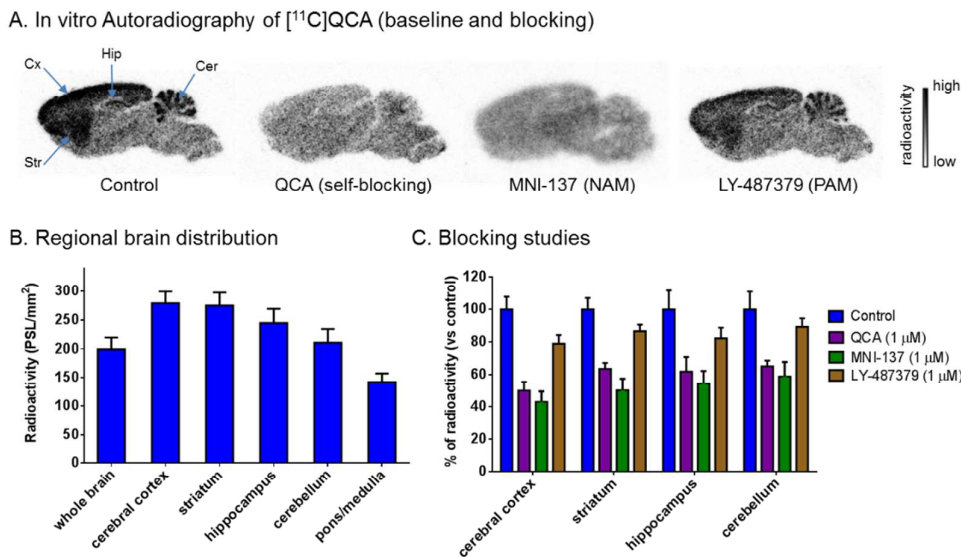


Figure 5. In vitro autoradiography of [¹¹C]QCA binding in rat brain sections. (A) Brain sections were treated with [¹¹C]QCA in the absence (baseline) or presence of QCA, MNI-137, LY-487379 (1 μM each). Cer, cerebellum; Hip, hippocampus; Cx, cortex; Str, striatum. (B) The radioactivity distribution was quantified in regional rat brain. The data are expressed as radioactivity per mm² (n = 4). (C) Blocking studies. The data are normalized to % of radioactivity vs control (n = 4).

PET imaging studies in normal rat brain. Dynamic PET acquisitions were carried out with [¹¹C]QCA in Sprague-Dawley rats for 60 min. Representative PET images (summed 0-60 min) in whole brain and time-activity curves are shown in **Figure 6**. The tracer [¹¹C]QCA showed limited brain uptake (ca. 0.3 SUV whole brain) in rat and no obvious washout (ratio of SUV_{5 min} / SUV_{90 min} = 1.1). Pretreatment with unlabeled QCA (1 mg/kg) failed to show significant reduction of brain uptake, likely attributed to low brain permeability and possible *in vivo* non-specific binding (**Figure 6C**). We next carried out radiometabolite analysis and PET imaging in PgP/Bcrp knockout mice to investigate possible reasons of limited CNS penetration.

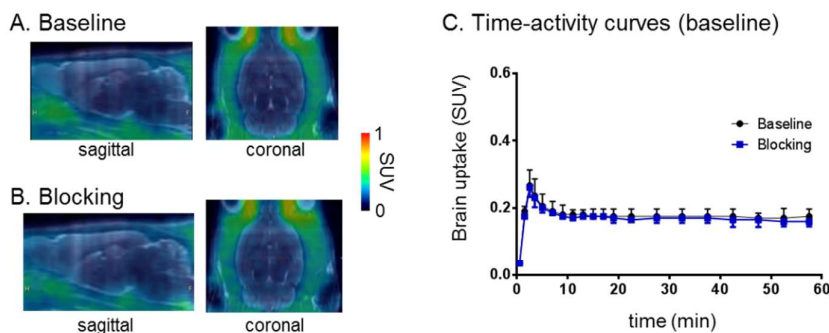


Figure 6. PET/MRI fused images of [^{11}C]QCA in rat brain: (A) baseline and (B) self-blocking with QCA (1 mg/kg). (C) Time-activity curves in whole brain under baseline and QCA self-blocking.

Radiometabolite analysis. To evaluate the in vivo stability of [^{11}C]QCA, radiometabolites in the plasma and brain homogenate of Sprague-Dawley rats were evaluated post-tracer injection. The percentages of unchanged [^{11}C]QCA and the corresponding radiometabolites, as determined by radio-HPLC, are shown in **Figure 7**. The fraction corresponding to unchanged [^{11}C]QCA in plasma was 93% at 5 min, 88% at 20 min and 79% at 60 min, respectively, with only one other more polar metabolite observed (Top three possible sites for the metabolism are predicted by SMARTCyp⁷⁵ and the results are listed as Table S3 in the supporting information). Analysis of rat brain homogenates in the same time interval showed unchanged [^{11}C]QCA was 78%, 41% and 34%, respectively, with the same radiometabolite as found in plasma. These results indicate that the resulting polar radiometabolite may be brain penetrant.

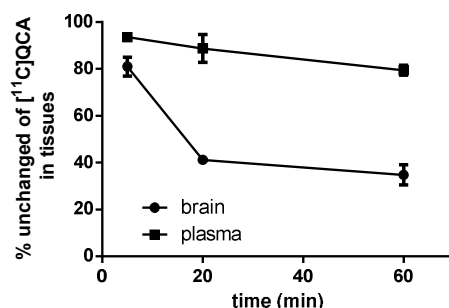


Figure 7. Percentages of unchanged [^{11}C]QCA in rat brain tissue and plasma ($n = 3$) at 5, 20 and 60 min post injection.

PET imaging studies in PgP/Bcrp knockout mice. Based on the results of in vitro autoradiography and in vivo PET studies on rat brain, we speculated that insufficient brain permeability of [^{11}C]QCA might be induced by ATP-binding cassette efflux transporters located at the blood-brain barrier,^{66,76-79} particularly, P-glycoprotein (PgP, ABCB1) and breast cancer resistance protein (Bcrp, ABCG2). To test this hypothesis, we carried out PET imaging studies of [^{11}C]QCA on wild-type and PgP/Bcrp knockout (ABCB1a/1b^{-/-}ABCG2^{-/-}) mice, and compared pharmacokinetic profiles, particularly brain uptake and clearance.

As shown in **Figure 8**, peak brain uptake in whole brain was *ca.* 0.8 SUV in PgP/Bcrp knockout mice, indicating a significant difference compared with that (*ca.* 0.3 SUV) of the wild-type mice. Whole brain uptake increased 130% in PgP/Bcrp knockout mice compared with that of wild-type mice (calculated based on area under curve). Therefore these results indicated that [^{11}C]QCA had intensive interactions with brain efflux pumps on the murine blood-brain barrier and is likely a PgP/Bcrp substrate in rodents.

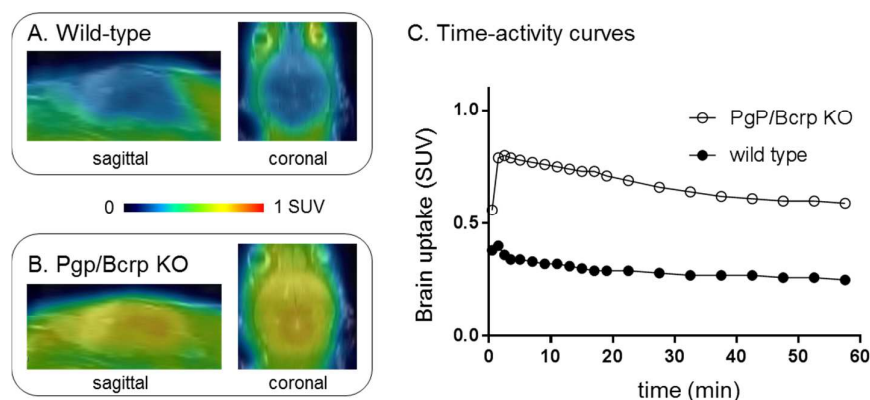


Figure 8. PET/MRI fused images in the whole brain of (A) wild-type and (B) Pgp/Bcrp knockout mouse. (C) Time-activity curves of whole brain in wildtype and Pgp/Bcrp knockout mouse after [^{11}C]QCA injection.

CONCLUSION

We have efficiently synthesized a focused library of NAMs targeting mGlu₂, and radiolabeled the most promising ligand, namely [^{11}C]QCA in good radiochemical yield, high radiochemical purity and high specific activity. The pharmacokinetic profile (ex vivo distribution, uptake and clearance), in vitro autoradiography, brain penetration, efflux pump and metabolism studies were evaluated to determine the suitability of [^{11}C]QCA as a mGlu₂ tracer. While [^{11}C]QCA is not likely pursued for in vivo mapping of mGlu₂ due to limited brain permeability, in vitro specific binding studies by autoradiography showed promise as a new chemotype for mGlu₂ tracer development. Further SAR studies of succinimidyl and/or quinoline carboxamide functionality are necessary to test Pgp/Bcrp efflux liability and to facilitate next generation tracer design with improved brain permeability. In-depth pharmacology evaluation is equally important to validate *in vivo* specificity using mGlu₂ knockout mice and/or mGlu₂-specific NAMs. Radiotracer's binding will also be evaluated under different agonist concentrations to characterize and select NAM- or PAM-based tracer for future clinical translation."

METHODS

Materials and Methods. General Consideration. All the chemicals employed in the syntheses were purchased from commercial vendors and used without further purification. Thin-layer chromatography (TLC) was conducted with 0.25 mm silica gel plates ($^{60}\text{F}_{254}$) and visualized by exposure to UV light (254 nm) or stained with potassium permanganate. Flash column chromatography was performed using silica gel (particle size 0.040-0.063 mm). H-Nuclear magnetic resonance (NMR) spectra were obtained on a 300 MHz on Bruker spectrometers and ^{13}C NMR spectra were obtained at 75 MHz. Chemical shifts (δ) are reported in ppm and coupling constants are reported in Hertz. The multiplicities are abbreviated as follows: s = singlet, d = doublet, t = triplet, q = quartet, quint = quintet, sext = sextet, sept = septet, m = multiplet, br = broad signal, dd = doublet of doublets. For

LC-MS/MS measurements, the ionization method is ESI using Agilent 6430 Triple Quad LC/MS. Lipophilicity was calculated by Pallas 3.4 ADME prediction software (CompDrug International, Inc., USA). The animal experiments were approved by the Institutional Animal Care and Use Committee of Massachusetts General Hospital or the Animal Ethics Committee at the National Institute of Radiological Sciences. DdY mice (male; 7 weeks, 34-36 g), Pgp/Bcrp knockout (Abcb1a/1b^{-/-}Abcg2^{-/-}; male; 17-18 weeks old; 31-33 g), wild-type (male; 17-18 weeks old; 30-32 g) FAB mice and Sprague-Dawley rats (male; 7 weeks; 210-230 g) were kept on a 12 h light/12 h dark cycle and were allowed food and water *ad libitum*.

Chemistry.

7-methylquinoline-2-carbonitrile (8). 7-methylquinoline (10 g, 57.9 mmol) was dissolved in dichloromethane (200 mL) in a round bottom flask with a stir bar. 3-Chloroperoxybenzoic acid (14.4 g, 75%, 75.33 mmol) was added in portions with ice bath. The mixture was stirred at room temperature overnight, then quenched with 400 mL 1N NaOH_(aq.) and extracted with dichloromethane (200 mL x 3). The combined organic layers were washed with saturated aqueous sodium bicarbonate, dried over MgSO₄ and concentrated to give 7-methylquinoline *N*-oxide. The crude product was used without further purification. To a solution of 7-methylquinoline *N*-oxide in dichloromethane (200 mL) was added trimethylsilyl cyanide (11.9g, 120.6 mmol) and dimethylcarbamoyl chloride (13.0 g 120.6 mmol). The mixture was stirred at room temperature overnight, then quenched with saturated sodium bicarbonate and extracted with dichloromethane (200 mL x 3). The combined organic layers were washed with saturated aqueous sodium chloride, dried over MgSO₄ and concentrated *in vacuo*. The residue was purified by flash chromatography on silica gel (hexanes to ethyl acetate gradient column) to yield the compound **8** as white solid (7.3 g, 74% over two steps). *R*_f = 0.3 (Hexanes/EtOAc = 20:1). ¹H NMR (400 MHz, CDCl₃) δ 8.27 (d, *J* = 8.3 Hz, 1H), 7.95 (s, 1H), 7.81 (d, *J* = 8.4 Hz, 1H), 7.66 (d, *J* = 8.3 Hz, 1H), 7.58 – 7.52 (m, 1H), 2.62 (s, 3H). ¹³C NMR (100 MHz, CDCl₃) δ 148.3, 142.1, 137.1, 133.3, 131.8, 128.6, 127.3, 126.8, 122.6, 117.5, 21.9.

4-chloro-7-methylquinoline-2-carbonitrile (9). Compound **8** (7.0 g, 41.6 mmol) was dissolved in dichloromethane (300 mL) in a round bottom flask with a stir bar. 3-Chloroperoxybenzoic acid (28.7 g, 75%, 124.8 mmol) was added in portions with ice bath. The mixture was stirred at 40°C for 3 h, then additional 3-chloroperoxybenzoic acid (28.7 g, 75%, 124.8 mmol) was added. The mixture was stirred at room temperature overnight, then quenched with 400 mL 1N NaOH_(aq.) and extracted with dichloromethane (200 mL x 3). The combined organic layers were washed with saturated aqueous sodium bicarbonate, dried over MgSO₄ and concentrated to give 4-chloro-7-methylquinoline-2-carbonitrile *N*-oxide. The crude product was used without further purification. To a solution of 4-chloro-7-methylquinoline-2-carbonitrile *N*-oxide in chloroform (200 mL) was added DMF (3.0 g, 41.3 mmol). Then POCl₃ (38.0 g, 247.6 mmol) was added in three portions at 70°C in 4 h. The mixture was stirred at 70 °C for 2 h before pour into iced water and extracted with dichloromethane (200 mL x 3). The combined organic layers were washed with saturated aqueous sodium chloride, dried over MgSO₄ and concentrated *in vacuo*. The residue was purified by flash chromatography on silica gel (hexanes to ethyl acetate gradient column) to yield the compound **9** as white solid (5.4 g, 64% over two steps). *R*_f = 0.3 (Hexanes/EtOAc =

20:1). ^1H NMR (400 MHz, CDCl_3) δ 8.17 (d, J = 8.6 Hz, 1H), 8.00 – 7.91 (m, 1H), 7.72 (s, 1H), 7.64 (dd, J = 8.7, 1.7 Hz, 1H), 2.62 (s, 3H). ^{13}C NMR (100 MHz, CDCl_3) δ 149.0, 143.7, 143.0, 133.1, 132.8, 129.2, 125.3, 123.8, 122.5, 116.7, 21.8.

7-(bromomethyl)-4-chloroquinoline-2-carbonitrile (10). To a solution of the compound **9** (1.17 g, 5.76 mmol) in CCl_4 (110 mL) under Ar was added *N*-bromosuccinimide (1.13 g, 6.33 mmol) and benzoyl peroxide (139.50 mg, 0.579 mmol). The mixture was stirred at 85°C for 4 h, then quenched with water (50 mL) and extracted with dichloromethane (100 mL x 3). The combined organic layers were washed with saturated aqueous sodium chloride, dried over MgSO_4 and concentrated *in vacuo*. The residue was purified by flash chromatography on silica gel (hexanes to ethyl acetate gradient column) to yield the compound **10** as white solid (60%, 967 mg). R_f = 0.2 (Hexanes/EtOAc = 20:1). ^1H NMR (400 MHz, CDCl_3) δ 8.29 (d, J = 8.6 Hz, 1H), 8.17 (s, 1H), 7.84 (d, J = 8.6 Hz, 1H), 7.80 (s, 1H), 4.68 (s, 2H). ^{13}C NMR (100 MHz, CDCl_3) δ 148.7, 144.0, 142.1, 133.8, 131.4, 129.8, 126.8, 125.1, 123.7, 116.4, 31.5.

4-chloro-7-((2,5-dioxopyrrolidin-1-yl)methyl)quinoline-2-carbonitrile (11). To a solution of the compound **10** (719 mg, 2.55 mmol) and succinimide (303 mg, 3.06 mmol) in DMF (15 mL) was added Cs_2CO_3 (1.66 g, 5.11 mmol). The mixture was stirred at room temperature for 0.5 h, then quenched with saturated aqueous KH_2PO_4 (40 mL) and extracted with ethyl acetate (40 mL x 3). The combined organic layers were washed with saturated aqueous sodium chloride, dried over MgSO_4 and concentrated *in vacuo*. The residue was purified by flash chromatography on silica gel (hexanes to ethyl acetate gradient column) to yield the compound **11** as white solid (80%, 612 mg). R_f = 0.2 (Hexanes/EtOAc = 1:1). ^1H NMR (400 MHz, CDCl_3) δ 8.25 (d, J = 8.7 Hz, 1H), 8.09 (s, 1H), 7.80 (d, J = 8.8 Hz, 1H), 7.77 (s, 1H), 4.92 (s, 2H), 2.81 (s, 4H). ^{13}C NMR (100 MHz, CDCl_3) δ 176.5, 148.7, 144.0, 140.0, 133.6, 130.9, 129.3, 126.6, 124.8, 123.4, 116.4, 41.8, 28.2.

7-((2,5-dioxopyrrolidin-1-yl)methyl)-4-(2-fluoro-4-methoxyphenyl)quinoline-2-carboxamide (QCA; 16). To a solution of the 2-fluoro-4-methoxyphenylboronic acid (54.4 mg, 0.320 mmol) and Na_2CO_3 (56.6 mg, 0.534 mmol) in 1,4-dioxane : water (v/v, 10/1, 1.8 mL) was added compound **11** (80.0 mg, 0.267 mmol) and $\text{Pd}(\text{PPh}_3)_4$ (30.9 mg, 0.0267 mmol) under Ar. The mixture was stirred at 100°C for 4 h, then quenched with water (3 mL) and extracted with ethyl acetate (5 mL x 3). The combined organic layers were washed with saturated aqueous sodium chloride, dried over MgSO_4 and concentrated *in vacuo*. The residue was used without further purification. To the residue solution in acetone : water (v/v, 2/1, 15 mL) was added sodium percarbonate (0.251 g, 1.60 mmol). The mixture was stirred at room temperature for 4h, then added ethyl acetate (5 mL) and extracted with ethyl acetate (5 mL x 3). The residue was purified by flash chromatography on silica gel (hexanes to ethyl acetate gradient column) to yield QCA (**16**) as white solid (42% for two steps, 55 mg). R_f = 0.2 (Hexanes/EtOAc = 1:3). ^1H NMR (300 MHz, $\text{DMSO}-d_6$) δ 8.02 (s, 1H), 8.01 (s, 1H), 7.97 (s, 1H), 7.82 (s, 1H), 7.69 – 7.56 (m, 2H), 7.46 (t, J = 8.6 Hz, 1H), 6.86 – 6.72 (m, 2H), 4.78 (s, 2H), 3.87 (s, 3H), 2.73 (s, 4H). ^{13}C NMR (75 MHz, $\text{DMSO}-d_6$) δ 178.1, 166.4, 161.9 (d, J = 11.0 Hz), 160.0 (d, J = 244.1 Hz), 150.8, 146.8, 143.7, 139.2, 132.6 (d, J = 4.9 Hz), 128.9, 128.3, 126.8, 126.3, 120.0, 116.7 (d, J = 15.9 Hz), 111.6, 102.4 (d, J = 25.4 Hz), 56.3, 41.6, 28.7.

7-((2,5-dioxopyrrolidin-1-yl)methyl)-4-(2-fluoro-4-hydroxyphenyl)quinoline-2-carboxamide (17). To a solution of the 2-fluoro-4-hydroxyphenylboronic acid (50 mg, 0.320 mmol) and Na_2CO_3 (56.6 mg, 0.534 mmol) in 1,4-dioxane : water (v/v, 10/1, 1.8 mL) was added

compound **11** (80.0 mg, 0.267 mmol) and Pd(PPh₃)₄ (30.9 mg, 0.0267 mmol) under Ar. The mixture was stirred at 100°C for 4 h, then quenched with water (3 mL) and extracted with ethyl acetate (5 mL x 3). The combined organic layers were washed with saturated aqueous sodium chloride, dried over MgSO₄ and concentrated *in vacuo*. The residue was used without further purification. To the residue solution in acetone : water (v/v, 2/1, 1.5 mL) was added sodium percarbonate (0.251 g, 1.60 mmol). The mixture was stirred at room temperature for 4 h, then added ethyl acetate (5 mL) and extracted with ethyl acetate (5 mL x 3). The residue was purified by flash chromatography on silica gel (hexanes to ethyl acetate gradient column) to yield the compound **13** as white solid (39% for two steps, 49 mg). *R*_f = 0.2 (Hexanes/EtOAc = 1:3). ¹H NMR (300 MHz, DMSO-*d*₆) δ 10.32 (s, 1H), 8.31 (s, 1H), 8.01 (s, 1H), 7.96 (s, 1H), 7.81 (s, 1H), 7.71 – 7.66 (m, 2H), 7.34 (t, *J* = 8.6 Hz, 1H), 6.86 – 6.72 (m, 2H), 4.78 (s, 2H), 2.73 (s, 4H). ¹³C NMR (75 MHz, DMSO-*d*₆) δ 177.6, 166.0, 159.6 (d, *J* = 243.7 Hz), 160.0 (d, *J* = 11.7 Hz), 150.3, 146.4, 143.6, 138.6, 132.2 (d, *J* = 5.0 Hz), 128.4, 127.9, 126.5, 126.0, 119.5, 114.7 (d, *J* = 15.7 Hz), 112.3, 103.0 (d, *J* = 24.1 Hz), 41.2, 28.2.

7-((2,5-dioxopyrrolidin-1-yl)methyl)-4-(2-fluoro-4-(2-fluoroethoxy)phenyl)quinoline-2-carboxamide (**FEQCA; 18**). To a solution of the 2-fluoro-4-hydroxyphenylboronic acid (50 mg, 0.320 mmol) and Na₂CO₃ (56.6 mg, 0.534 mmol) in 1,4-dioxane : water (v/v, 10/1, 1.8 mL) was added compound **11** (80.0 mg, 0.267 mmol) and Pd(PPh₃)₄ (30.9 mg, 0.0267 mmol) under Ar. The mixture was stirred at 100°C for 4 h, then quenched with water (3 mL) and extracted with ethyl acetate (5 mL x 3). The combined organic layers were washed with saturated aqueous sodium chloride, dried over MgSO₄ and concentrated *in vacuo*. The residue was used without further purification. To the residue solution in DMF (1.5 mL) was added 1-fluoro-2-iodoethane (112 mg, 0.640 mmol) and Cs₂CO₃ (209 mg, 0.640 mmol). The mixture was stirred at room temperature overnight, then quenched with saturated aqueous KH₂PO₄ (5 mL). The combined organic layers were washed with saturated aqueous sodium chloride, dried over MgSO₄ and concentrated *in vacuo*. The residue was purified by flash chromatography on silica gel (hexanes to ethyl acetate gradient column) to yield the compound **14** as white solid (45% for two steps, 50.6 mg) and used directly in the next step. To the solution of compound **14** (42.1 mg, 0.1 mmol) in acetone : water (v/v, 2/1, 2 mL) was added sodium percarbonate (78 mg, 0.50 mmol). The mixture was stirred at room temperature for 4h, then added ethyl acetate (5 mL) and extracted with ethyl acetate (5 mL x 3). The residue was purified by flash chromatography on silica gel (hexanes to ethyl acetate gradient column) to yield FEQCA (**18**) as white solid (60%, 26.3 mg). *R*_f = 0.2 (Hexanes/EtOAc = 1:3). ¹H NMR (300 MHz, DMSO-*d*₆) δ 8.34 (s, 1H), 8.03 (s, 1H), 7.99 (s, 1H), 7.83 (s, 1H), 7.69 – 7.59 (m, 2H), 7.47 (t, *J* = 8.6 Hz, 1H), 7.45 – 7.02 (m, 2H), 4.79 (dt, *J* = 47.9, 3.5 Hz), 4.78 (s, 2H), 4.37 (dt, *J* = 30.0, 3.5 Hz), 2.73 (s, 4H). ¹³C NMR (75 MHz, DMSO-*d*₆) δ 178.1, 166.4, 160.0 (d, *J* = 243.8 Hz), 160.6 (d, *J* = 11.1 Hz), 150.7, 146.8, 143.6, 139.2, 134.7 (d, *J* = 4.7 Hz), 128.9, 128.4, 126.7, 126.3, 120.0, 117.1 (d, *J* = 15.8 Hz), 112.0, 103.0 (d, *J* = 25.7 Hz), 82.4 (d, *J* = 165.6 Hz), 68.2 (d, *J* = 18.8 Hz), 41.6, 28.6.

7-((2,5-dioxopyrrolidin-1-yl)methyl)-4-(2-fluoro-4-(3-fluoropropoxy)phenyl)quinoline-2-carboxamide (**FPQCA; 19**). To a solution of the 2-fluoro-4-hydroxyphenylboronic acid (50 mg, 0.320 mmol) and Na₂CO₃ (56.6 mg, 0.534 mmol) in 1,4-dioxane : water (v/v, 10/1, 1.8 mL) was added compound **11** (80.0 mg, 0.267 mmol) and Pd(PPh₃)₄ (30.9 mg, 0.0267 mmol) under Ar. The mixture was stirred at 100°C for 4 h, then quenched with water (3 mL) and

extracted with ethyl acetate (5 mL x 3). The combined organic layers were washed with saturated aqueous sodium chloride, dried over MgSO_4 and concentrated *in vacuo*. The residue was used without further purification. To the residue solution in DMF (1.5 mL) was added 1-fluoro-3-iodopropane (120 mg, 0.640 mmol) and Cs_2CO_3 (209 mg, 0.640 mmol). The mixture was stirred at room temperature overnight, then quenched with saturated aqueous KH_2PO_4 (5 mL). The combined organic layers were washed with saturated aqueous sodium chloride, dried over MgSO_4 and concentrated *in vacuo*. The residue was purified by flash chromatography on silica gel (hexanes to ethyl acetate gradient column) to yield the compound **15** as white solid (47% for two steps, 54.6 mg) and used directly in the next step. To the solution of compound **15** (43.6 mg, 0.1 mmol) in acetone : water (v/v, 2/1, 2 mL) was added sodium percarbonate (78 mg, 0.50 mmol). The mixture was stirred at room temperature for 4 h, then added ethyl acetate (5 mL) and extracted with ethyl acetate (5 mL x 3). The residue was purified by flash chromatography on silica gel (hexanes to ethyl acetate gradient column) to yield FPQCA (**19**) as white solid (53%, 24 mg). $R_f = 0.2$ (Hexanes/EtOAc = 1:3). ^1H NMR (300 MHz, $\text{DMSO}-d_6$) δ 8.33 (s, 1H), 8.02 (s, 1H), 7.97 (s, 1H), 7.82 (s, 1H), 7.69 – 7.57 (m, 2H), 7.46 (t, $J=8.6$ Hz, 1H), 7.45 – 7.02 (m, 2H), 4.78 (s, 2H), 4.63 (dt, $J=47.3$, 5.9 Hz), 4.19 (t, $J=6.3$ Hz), 2.73 (s, 4H), 2.22 – 2.07 (m, 2H). ^{13}C NMR (75 MHz, $\text{DMSO}-d_6$) δ 178.1, 166.4, 160.0(d, $J=244.4$ Hz), 161.0 (d, $J=12.5$ Hz), 150.7, 146.8, 143.7, 139.2, 132.6 (d, $J=5.0$ Hz), 128.9, 128.3, 126.8, 126.3, 120.0, 116.8 (d, $J=16.0$ Hz), 112.0, 102.9 (d, $J=25.6$ Hz), 81.2 (d, $J=160.7$ Hz), 64.7 (d, $J=5.3$ Hz), 41.6, 64.7 (d, $J=19.6$ Hz), 28.6.

Pharmacology.

Cell line generation and thallium flux assays. In order to generate human mGlu_2 and mGlu_3 stable cell lines to be used for thallium flux assays, human mGlu_2 and mGlu_3 were prepared by PCR amplification of the entire coding sequence of each receptor and cloning into pIRES puro 3 (Invitrogen). For mGlu_2 and mGlu_3 , the cloning sites were NheI/NotI . HEK GIRK cells, generously provided by Lily Jan (University of California San Francisco, San Francisco, CA), were transfected with 24 μg of DNA using Eugene6 (Promega), stable transfectants were selected with 1000 ng/mL puromycin dihydrochloride (Sigma-Aldrich, St. Louis, MO), and polyclonal human mGlu_2 GIRK and mGlu_3 GIRK cell lines were established. Cells were maintained following selection in 45% DMEM, 45% Ham's F12, 10% FBS, 100 units/mL penicillin/streptomycin, 20 mM HEPES, pH 7.3, 1 mM sodium pyruvate, 2 mM glutamine, 700 $\mu\text{g}/\text{mL}$ G418 (Mediatech, Inc., Herndon, VA), and 600 $\mu\text{g}/\text{mL}$ puromycin (growth media) at 37°C in the presence of 5% CO_2 . All cell culture reagents were purchased from Invitrogen Corp. (Carlsbad, CA) unless otherwise noted.

Human mGlu_2 and mGlu_3 thallium flux in vitro assays. Compound activity at mGlu_2 and mGlu_3 was assessed using thallium flux through GIRK channels, a method that has been described in detail.^{80,81} Briefly, cells were plated into 384-well, black-walled, clear-bottomed poly-D-lysine-coated plates at a density of 15,000 cells/20 $\mu\text{L}/\text{well}$ in DMEM containing 10% dialyzed FBS, 20 mM HEPES, and 100 units/mL penicillin/streptomycin (assay media). Plated cells were incubated overnight at 37°C in the presence of 5% CO_2 . The following day, the medium was exchanged from the cells to assay buffer [Hanks' balanced salt solution (Invitrogen) containing 20 mM HEPES, pH 7.3] using an ELX405 microplate washer (BioTek), leaving 20 $\mu\text{L}/\text{well}$, followed by the addition of 20 $\mu\text{L}/\text{well}$ FluoZin2-AM (330 nM

final concentration) indicator dye (Invitrogen; prepared as a stock in DMSO and mixed in a 1:1 ratio with Pluronic acid F-127) in assay buffer. Cells were incubated for 1 h at room temperature, and the dye exchanged to assay buffer using an ELX405, leaving 20 μ L/well. For concentration-response curve experiments, compounds were serially diluted 1:3 into 10 point concentration response curves and were transferred to daughter plates using an Echo acoustic plate reformatter (Labcyte, Sunnyvale, CA). Test compounds were diluted to 2 times their final desired concentration in assay buffer (0.3% DMSO final concentration). Agonists were diluted in thallium buffer [125 mM sodium bicarbonate (added fresh the morning of the experiment), 1 mM magnesium sulfate, 1.8 mM calcium sulfate, 5 mM glucose, 12 mM thallium sulfate, and 10 mM HEPES, pH 7.3] at 5 times the final concentration to be assayed. Cell plates and compound plates were loaded onto a kinetic imaging plate reader (FDSS 6000 or 7000; Hamamatsu Corporation, Bridgewater, NJ). Appropriate baseline readings were taken (10 images at 1 Hz; excitation, 470 ± 20 nm; emission, 540 ± 30 nm) and test compounds were added in a 20 μ L volume and incubated for approximately 1 hour at room temperature before the addition of 10 μ L of thallium buffer with or without an EC₈₀ concentration of the agonist glutamate for potency evaluation experiments or with a full concentration-response of glutamate for Schild analysis experiments. After the addition of agonist, data were collected for approximately an additional 2.5 min. Data were analyzed using Excel (Microsoft Corp, Redmond, WA). The slope of the fluorescence increase beginning 5 s after thallium/agonist addition and ending 15 s after thallium/agonist addition was calculated, corrected to vehicle and maximal agonist control slope values, and plotted in using either XLfit (ID Business Solutions Ltd) or Prism software (GraphPad Software, San Diego, CA) to generate concentration-response curves. Potencies were calculated from fits using a four-point parameter logistic equation.

Measurement of physicochemical properties.

Measurement of partition coefficient (LogP) ("shake flask method"). The measurement of LogP value was performed by mixing test compound (50 μ L, 20 μ M in DMSO) with *n*-octanol (475 μ L) and water (475 μ L) in a test tube. The *n*-octanol and water were pre-saturated with each other before use. The tube was vortexed for 1 min before shaken at 37°C overnight. Water phase and *n*-octanol phase (200 μ L each) were aliquoted. The amount of the test compound in each phase was determined by LC-MS/MS (Agilent 6430 Triple Quad LC/MS). The LogP was calculated by Log [ratio between the amount of test compound in *n*-octanol and water solution]. The procedure was repeated triplicate and the value was shown in Table 1.

Measurement of pH stability. The stability of compounds in buffer solutions was measured using a HPLC method adapted from our previous protocol.⁸² Briefly, testing compounds **16**, **18-19** (0.25 μ mol) were each dissolved in 1 mL DMSO to make a stock solution. An aliquot (50 μ L stock solution) was mixed with phosphate buffer (950 μ L, 20 mM, pH 7.4), boric acid-KCl-NaOH buffer (950 μ L, 20 mM, pH 9.4) or sodium acetate-KCl-HCl buffer (950 μ L, 20 mM, pH 5.0) and incubated for 1 h at 37 °C. The percentage of the unchanged compound was monitored by HPLC (Luna analytical column, 4.6 x 250 mm, 5 μ m, CH₃CN / H₂O + 0.1% TFA).

Measurement of plasma stability. The stability of candidate compounds in rat serum was measured using a literature method.⁸³ Briefly, the test was performed by mixing a candidate

compound (10 μ L, 10 μ M in DMSO stock solution) with 250 μ L aliquot of rat serum (Abcam, Inc. No. ab7488) in a test tube. The tube was vortexed before incubated at 37 °C for 60 min. The reaction was quenched by the addition of 250 μ L ice-cold CH₃CN, followed by centrifuge at 10,000 \times g for 10 min. The amount of the test compound was quantified by LC-MS/MS (Agilent 6430 Triple Quad LC/MS). The percentage remaining was calculated by (peak area at 60 min) / (peak area at 0 min) \times 100%. The procedure was repeated at least triplicate and diltiazem was used as a positive control.

Measurement of liver microsomal stability. The stability of candidate compounds in liver microsomes was measured using a literature method.⁸⁴ Briefly, the test was performed by mixing a candidate compound (0.5 μ L, 2 mM in DMSO stock solution) with PBS (432 μ L) and 13 μ L aliquot of Sprague-Dawley rat liver microsomes (Sigma-Aldrich, No. M9066) in a test tube. The tube was vortexed before shaken at 37 °C for 5 min, followed by the addition of NADPH (50 μ L, 10 mM in PBS stock solution). The mixture was incubated at 37 °C for 60 min, and quenched by the addition of 250 μ L ice-cold CH₃CN and centrifuge at 10,000 \times g for 10 min. The amount of the test compound was quantified by LC-MS/MS (Agilent 6430 Triple Quad LC/MS). The percentage remaining was calculated by (peak area at 60 min) / (peak area at 0 min) \times 100%. The procedure was repeated at least triplicate and verapamil was used as a positive control.

Radiochemistry. *Radiolabeling of [¹¹C]QCA.* [¹¹C]Methyl iodide ([¹¹C]CH₃I) was synthesized from cyclotron-produced [¹¹C]CO₂, which was produced by ¹⁴N(p, α)¹¹C nuclear reaction. Briefly, [¹¹C]CO₂ was bubbled into a solution of LiAlH₄ (0.4 M in THF, 300 μ L). After evaporation, the remaining reaction mixture was treated with hydroiodic acid (57% aqueous solution, 300 μ L). The resulting [¹¹C]CH₃I was transferred under helium gas with heating into a pre-cooled (-15 to -20 °C) reaction vessel containing precursor 17 (0.5 mg), NaOH (2.5 μ L, 0.5 M) and anhydrous DMF (300 μ L). After the radioactivity reached a plateau during transfer, the reaction vessel was warmed to 80 °C and maintained for 5 min. CH₃CN / H₂O + 0.1% Et₃N (v/v, 4/6, 0.5 mL) was added to the reaction mixture, which was then injected to a semi-preparative HPLC system. HPLC purification was completed on a Capcell Pak UG80 C18 column (10 mm ID \times 250 mm) using a mobile phase of CH₃CN / H₂O + 0.1% Et₃N (v/v, 4/6) at a flowrate of 6.0 mL/min. The retention time for [¹¹C]QCA was 9.5 min. The radioactive fraction corresponding to the desired product was collected in a sterile flask, evaporated to dryness *in vacuo*, and reformulated in a saline solution (3 mL) containing 100 μ L of 25% ascorbic acid in sterile water and 100 μ L of 20% Tween[®] 80 in ethanol. (Note: We added ascorbic acid to prevent potential radiolysis and Tween[®] 80 to improve aqueous solubility.) The synthesis time was *ca.* 30 min from end-of-bombardment. Radiochemical and chemical purity were measured by analytical HPLC (Capcell Pak UG80 C18, 4.6 mm ID \times 250 mm, UV at 254 nm; CH₃CN / H₂O + 0.1% Et₃N (v/v, 4/6) at a flowrate of 1.2 mL/min). The identity of [¹¹C]QCA was confirmed by the co-injection with unlabeled QCA. Radiochemical yield was 46% decay-corrected based on [¹¹C]CO₂ with >99% radiochemical purity and greater than 2 Ci/ μ mol specific activity.

Ex vivo biodistribution in mice. A solution of [¹¹C]QCA (50 μ Ci / 150-200 μ L) was injected into DdY mice via the tail vein. These mice (n = 5, each time point) were sacrificed at 1, 5, 15, 30 and 60 min post tracer injection. Major organs, including whole brain, heart,

liver, lung, spleen, kidneys, small intestine (including contents), muscle, testes, and blood samples were quickly harvested and weighted. The radioactivity present in these tissues was measured using a gamma counter (PerkinElmer, USA), and all radioactivity measurements were automatically decay corrected based on half-life of ^{11}C . The results are expressed as the percentage of injected dose per gram of wet tissue (% ID/g) or standardized uptake value (SUV).

In vitro autoradiography. Rat brain was cut into 20 μM sections and stored at -80°C until they were used for experiment. The rat brain sections were pre-incubated with Tris-HCl buffer (50 mM), MgCl_2 (1.2 mM) and CaCl_2 (2 mM) solution for 20 min at ambient temperature, followed by incubation with $[^{11}\text{C}]\text{QCA}$ (0.48 nM). For blocking studies, unlabeled QCA (1 μM) was added to incubation solution in advance to determine the specificity of radioligand binding. After incubation, brain sections were rinsed with ice-cold buffer three times for 2 min, dipped in cold distilled water for 10 sec. The brain sections were dried with cold air, then placed on imaging plates (BAS-MS2025, GE Healthcare, NJ, USA) for optimized contact periods. Autoradiograms were obtained and ROIs were carefully drawn with the reference of naked-eye observation. Radioactivity was expressed as photostimulated luminescence values per unit area (PSL/ mm^2) and measured by a Bio-Imaging analyzer system (BAS5000, Fujifilm).

Small-animal PET imaging studies. PET scans were acquired by an Inveon PET scanner (Siemens Medical Solutions, Knoxville, TN, USA). Sprague-Dawley rats were kept under anesthesia with 1-2% (v/v) isoflurane during the scan. The radiotracer (ca. 1 mCi / 150-200 μL) was injected via a preinstalled catheter via tail vein. A dynamic scan in 3D list mode was acquired for 60 min. For pretreatment studies, QCA (1 mg/kg) pre-dissolved in 300 μL saline containing 10% ethanol and 5% Tween[®] 80 was injected at 30 min via the tail vein catheter before the injection of $[^{11}\text{C}]\text{QCA}$.

As we previously reported,^{78,79} the PET dynamic images were reconstructed using ASIPro VW software (Analysis Tools and System Setup/Diagnostics Tool, Siemens Medical Solutions). Volumes of interest, including the whole brain, cerebral cortex, cerebellum, striatum, thalamus and pons were placed using ASIPro software. The radioactivity was decay-corrected and expressed as the standardized uptake value. $\text{SUV} = (\text{radioactivity per mL tissue} / \text{injected radioactivity}) \times \text{body weight}$.

Radiometabolite analysis. Following the intravenous injection of $[^{11}\text{C}]\text{QCA}$, Sprague-Dawley rats were sacrificed at 5, 20 and 60 min ($n = 3$ each time point). Blood and whole brain samples were quickly removed and the blood samples were centrifuged at 15,000 $\times g$ for 2 min at 4°C to separate the plasma. The supernatant (0.5 mL) was then collected in a test tube containing CH_3CN (0.5 mL) and the resulting mixture was vortexed for 15s and centrifuged at 15,000 $\times g$ for 2 min for deproteinization. The rat brain was homogenized in an ice-cooled $\text{CH}_3\text{CN}/\text{H}_2\text{O}$ (1 mL, 1/1, v/v) solution. The homogenate was centrifuged at 150,000 rpm for 2 min at 4°C and the supernatant was collected. The recovery of radioactivity into the supernatant was $> 90\%$ based on the total radioactivity in the brain homogenate.

An aliquot of the supernatant (100 μL) obtained from the plasma or brain homogenate was injected into the radio-HPLC system, and analyzed using a Capcell Pak UG80 C18

column (4.6 mm ID × 250 mm) in a mobile phase of CH₃CN / H₂O + 0.1% Et₃N (v/v, 45/55) at a flowrate of 1.0 mL/min. The retention time of [¹¹C]QCA is 7.8 min. The percentage of [¹¹C]QCA to total radioactivity (corrected for decay) on the HPLC charts was calculated as (peak area for [¹¹C]QCA/total peak area) × 100.

ASSOCIATED CONTENT

Retrosynthetic analysis; Characterization of all new compounds and NMR spectra; assay methods; GPCRome data sheet. This material is available free of charge via the Internet at <http://pubs.acs.org>.

AUTHOR INFORMATION

Corresponding Author

* Tel: +81 433 823 709. Fax: +81-43-206-3261. E-mail: zhang.ming-rong@qst.go.jp.

* Tel: +1 617 726 6107. Fax: +1 617 726 6165. E-mail: liang.steven@mgh.harvard.edu.

Author Contributions

The manuscript was written through contributions of all authors. All authors have given approval to the final version of the manuscript. [#]X. Zhang and K. Kumata contributed equally.

Notes

The authors declare no competing financial interest.

ACKNOWLEDGEMENTS

We would like to thank the staff at the radiochemistry program, Massachusetts General Hospital, MA, USA and National Institutes for Quantum and Radiological Science and Technology, National Institute of Radiological Sciences, Chiba, Japan for their support. We thank the National Institute of Mental Health's Psychoactive Drug Screening Program (NIMH PDSP) for the compound screening. The NIMH PDSP is directed by Bryan L. Roth MD, PhD at the University of North Carolina at Chapel Hill and Project Officer Jamie Driscoll at NIMH, Bethesda MD, USA. We also thank Drs. Thomas J. Brady and Lei Zhang for helpful discussion. X.Z. is supported by China Scholarship Council Fellowship (201606200041). N.D.P.C. is supported by a National Institute of Mental Health grant (R01-MH106865). S.H.L. is a recipient of NIH career development award from the National Institute on Drug Abuse (DA038000).

ABBREVIATIONS

PET, positron emission tomography; mGlu₂, metabotropic glutamate receptor 2; PAM, positive allosteric modulator; NAM, negative allosteric modulator; NBS, *N*-bromosuccinimide; AIBN, 2,2-azobis(2-methylpropionitrile); mCPBA, *meta*-chloroperbenzoic acid; DCM, dichloromethane; DMF, dimethylformamide; ADME, absorption, distribution, metabolism and excretion; MPO, multiparameter optimization; SUV, standardized uptake value; TAC, time-activity curve; %ID/g, percentage of injected dose per gram of wet tissue; KO, knockout; PgP, P-glycoprotein; Bcrp, breast cancer resistance protein.

REFERENCES

1. Nakanishi, S. Molecular diversity of glutamate receptors and implications for brain function. *Science* **258**, 597-603 (1992).
2. Kew, J.N. & Kemp, J.A. Ionotropic and metabotropic glutamate receptor structure and pharmacology. *Psychopharmacology* **179**, 4-29 (2005).
3. Bowie, D. Ionotropic glutamate receptors & CNS disorders. *CNS Neurol Disord Drug Targets* **7**, 129-143 (2008).
4. Traynelis, S.F., Wollmuth, L.P., McBain, C.J., Menniti, F.S., Vance, K.M., Ogden, K.K., Hansen, K.B., Yuan, H., Myers, S.J. & Dingledine, R. Glutamate receptor ion channels: structure, regulation, and function. *Pharmacol Rev* **62**, 405-496 (2010).
5. Lau, A. & Tymianski, M. Glutamate receptors, neurotoxicity and neurodegeneration. *Pflugers Arch* **460**, 525-542 (2010).
6. Niciu, M.J., Kelmendi, B. & Sanacora, G. Overview of glutamatergic neurotransmission in the nervous system. *Pharmacol Biochem Behav* **100**, 656-664 (2012).
7. Niswender, C.M. & Conn, P.J. Metabotropic glutamate receptors: physiology, pharmacology, and disease. *Annu Rev Pharmacol Toxicol* **50**, 295-322 (2010).
8. Testa, C.M., Friberg, I.K., Weiss, S.W. & Standaert, D.G. Immunohistochemical localization of metabotropic glutamate receptors mGluR_{1a} and mGluR_{2/3} in the rat basal ganglia. *J Comp Neurol* **390**, 5-19 (1998).
9. Schoepp, D.D. Unveiling the functions of presynaptic metabotropic glutamate receptors in the central nervous system. *J Pharmacol Exp Ther* **299**, 12-20 (2001).
10. Ohishi, H., Shigemoto, R., Nakanishi, S. & Mizuno, N. Distribution of the messenger RNA for a metabotropic glutamate receptor, mGluR₂, in the central nervous system of the rat. *Neuroscience* **53**, 1009-1018 (1993).
11. Ohishi, H., Ogawa-Meguro, R., Shigemoto, R., Kaneko, T., Nakanishi, S. & Mizuno, N. Immunohistochemical localization of metabotropic glutamate receptors, mGluR₂ and mGluR₃, in rat cerebellar cortex. *Neuron* **13**, 55-66 (1994).
12. Ohishi, H., Neki, A. & Mizuno, N. Distribution of a metabotropic glutamate receptor, mGluR₂, in the central nervous system of the rat and mouse: an immunohistochemical study with a monoclonal antibody. *Neurosci Res* **30**, 65-82 (1998).
13. Richards, G., Messer, J., Malherbe, P., Pink, R., Brockhaus, M., Stadler, H., Wichmann, J., Schaffhauser, H. & Mutel, V. Distribution and abundance of metabotropic glutamate receptor subtype 2 in rat brain revealed by [³H]LY354740 binding in vitro and quantitative radioautography: Correlation with the sites of synthesis, expression, and agonist stimulation of [³⁵S]GTPγS binding. *J Comp Neurol* **487**, 15-27 (2005).
14. Wright, R.A., Johnson, B.G., Zhang, C., Salhoff, C., Kingston, A.E., Calligaro, D.O., Monn, J.A., Schoepp, D.D. & Marek, G.J. CNS distribution of metabotropic glutamate 2 and 3 receptors: transgenic mice and [³H]LY459477 autoradiography. *Neuropharmacology* **66**, 89-98 (2013).

15. Hovelso, N., Sotty, F., Montezinho, L.P., Pinheiro, P.S., Herrik, K.F. & Mork, A. Therapeutic potential of metabotropic glutamate receptor modulators. *Curr Neuroparmacol* **10**, 12-48 (2012).
16. Soto, D., Altafaj, X., Sindreu, C. & Bayes, A. Glutamate receptor mutations in psychiatric and neurodevelopmental disorders. *Commun Integr Biol* **7**, 6 (2014).
17. Golubeva, A.V., Moloney, R.D., O'Connor, R.M., Dinan, T.G. & Cryan, J.F. Metabotropic Glutamate Receptors in Central Nervous System Diseases. *Curr Drug Targets* **17**, 538-616 (2016).
18. Muguruza, C., Meana, J.J. & Callado, L.F. Group II Metabotropic Glutamate Receptors as Targets for Novel Antipsychotic Drugs. *Front Pharmacol* **7**(2016).
19. Ribeiro, F.M., Vieira, L.B., Pires, R.G., Olmo, R.P. & Ferguson, S.S. Metabotropic glutamate receptors and neurodegenerative diseases. *Pharmacol Res* **115**, 179-191 (2017).
20. Vaidya, A., Jain, S., Jain, A.K., Agrawal, A., Kashaw, S.K., Jain, S.K. & Agrawal, R.K. Metabotropic glutamate receptors: a review on prospectives and therapeutic aspects. *Mini Rev Med Chem* **13**, 1967-1981 (2013).
21. Clewa, R.M. & Olive, M.F. mGlu receptors and drug addiction. *Wiley Interdiscip Rev Membr Transp Signal* **1**, 281-295 (2012).
22. Pomierny-Chamiolo, L., Rup, K., Pomierny, B., Niedzielska, E., Kalivas, P.W. & Filip, M. Metabotropic glutamatergic receptors and their ligands in drug addiction. *Pharmacol Ther* **142**, 281-305 (2014).
23. Kalivas, P.W. & Volkow, N.D. New medications for drug addiction hiding in glutamatergic neuroplasticity. *Mol Psychiatry* **16**, 974-986 (2011).
24. Chiechio, S. & Nicoletti, F. Metabotropic glutamate receptors and the control of chronic pain. *Curr Opin Pharmacol* **12**, 28-34 (2012).
25. Campo, B., Kalinichev, M., Lambeng, N., El Yacoubi, M., Royer-Urios, I., Schneider, M., Legrand, C., Parron, D., Girard, F., Bessif, A., Poli, S., Vaugeois, J.M., Le Poul, E. & Celanire, S. Characterization of an mGluR_{2/3} negative allosteric modulator in rodent models of depression. *J Neurogenet* **25**, 152-166 (2011).
26. Dwyer, J.M., Lepack, A.E. & Duman, R.S. mGluR_{2/3} blockade produces rapid and long-lasting reversal of anhedonia caused by chronic stress exposure. *J Mol Psychiatry* **1**, 15 (2013).
27. Conn, P.J., Lindsley, C.W. & Jones, C.K. Activation of metabotropic glutamate receptors as a novel approach for the treatment of schizophrenia. *Trends Pharmacol Sci* **30**, 25-31 (2009).
28. Dickerson, J.W. & Conn, P.J. Therapeutic potential of targeting metabotropic glutamate receptors for Parkinson's disease. *Neurodegener Dis Manag* **2**, 221-232 (2012).
29. Samadi, P., Rajput, A., Calon, F., Grégoire, L., Hornykiewicz, O., Rajput, A.H. & Di Paolo, T. Metabotropic Glutamate Receptor II in the Brains of Parkinsonian Patients. *J Neuropathol Exp Neurol* **68**, 374-382 (2009).

30. Lee, H.G., Zhu, X., O'Neill, M.J., Webber, K., Casadesus, G., Marlatt, M., Raina, A.K., Perry, G. & Smith, M.A. The role of metabotropic glutamate receptors in Alzheimer's disease. *Acta Neurobiol Exp* **64**, 89-98 (2004).
31. Celanire, S., Sebbat, I., Wichmann, J., Mayer, S., Schann, S. & Gatti, S. Novel metabotropic glutamate receptor 2/3 antagonists and their therapeutic applications: a patent review (2005 - present). *Expert Opin Ther Pat* **25**, 69-90 (2015).
32. Melancon, B.J., Hopkins, C.R., Wood, M.R., Emmitte, K.A., Niswender, C.M., Christopoulos, A., Conn, P.J. & Lindsley, C.W. Allosteric modulation of seven transmembrane spanning receptors: theory, practice, and opportunities for central nervous system drug discovery. *J Med Chem* **55**, 1445-1464 (2012).
33. Lindsley, C.W., Emmitte, K.A., Hopkins, C.R., Bridges, T.M., Gregory, K.J., Niswender, C.M. & Conn, P.J. Practical Strategies and Concepts in GPCR Allosteric Modulator Discovery: Recent Advances with Metabotropic Glutamate Receptors. *Chem Rev* **116**, 6707-6741 (2016).
34. Trabanco, A.A. & Cid, J.M. mGluR2 positive allosteric modulators: a patent review (2009 - present). *Expert Opin Ther Pat* **23**, 629-647 (2013).
35. Felts, A.S., Rodriguez, A.L., Smith, K.A., Engers, J.L., Morrison, R.D., Byers, F.W., Blobaum, A.L., Locuson, C.W., Chang, S., Venable, D.F., Niswender, C.M., Daniels, J.S., Conn, P.J., Lindsley, C.W. & Emmitte, K.A. Design of 4-Oxo-1-aryl-1,4-dihydroquinoline-3-carboxamides as Selective Negative Allosteric Modulators of Metabotropic Glutamate Receptor Subtype 2. *J Med Chem* **58**, 9027-9040 (2015).
36. Fowler, J.S. & Wolf, A.P. Working against Time: Rapid Radiotracer Synthesis and Imaging the Human Brain. *Acc Chem Res* **30**, 181-188 (1997).
37. Phelps, M.E. Positron emission tomography provides molecular imaging of biological processes. *Proc Natl Acad Sci* **97**, 9226-9233 (2000).
38. Lee, C.-M. & Farde, L. Using positron emission tomography to facilitate CNS drug development. *Trends Pharmacol Sci* **27**, 310-316 (2006).
39. Willmann, J.K., van Bruggen, N., Dinkelborg, L.M. & Gambhir, S.S. Molecular imaging in drug development. *Nature reviews. Drug discovery* **7**, 591-607 (2008).
40. Sobrio, F. Radiosynthesis of carbon-11 and fluorine-18 labelled radiotracers to image the ionotropic and metabotropic glutamate receptors. *J Labelled Comp Radiopharm* **56**, 180-186 (2013).
41. Fuchigami, T., Nakayama, M. & Yoshida, S. Development of PET and SPECT Probes for Glutamate Receptors. *Scientific World J*, 19 (2015).
42. Mu, L. & Ametamey, S.M. Current Radioligands for the PET Imaging of Metabotropic Glutamate Receptors. in *PET and SPECT of Neurobiological Systems* (eds. Dierckx, R.A.J.O., Otte, A., de Vries, E.F.J., van Waarde, A. & Luiten, P.G.M.) 409-443 (Springer Berlin Heidelberg, Berlin, Heidelberg, 2014).
43. Zhang, Z. & Brownell, A.-L. Imaging of Metabotropic Glutamate Receptors (mGluRs). in *Neuroimaging - Clinical Applications* (ed. Bright, P.P.) DOI: 10.5772/23714 (2012).

- 1
2
3 44. Li, D., Shan, H., Conti, P. & Li, Z. PET imaging of metabotropic glutamate receptor
4 subtype 5 (mGluR5). *Am J Nucl Med Mol Imaging* **2**, 29-32 (2012).
5
6 45. Li, S. & Huang, Y. In vivo imaging of the metabotropic glutamate receptor 1
7 (mGluR1) with positron emission tomography: recent advance and perspective. *Curr*
8 *Med Chem* **21**, 113-123 (2014).
9
10 46. Wang, J.-Q., Kuruppu, D. & Brownell, A.-L. Radiosynthesis of the mGluR_{2/3} PET
11 tracer (S,S,S)-2-(2-carboxycyclopropyl)-2-(4-[¹¹C]methoxyphenethyl)glycine
12 dimethyl ester ([¹¹C]CMG). *J Nucl Med* **49**, 286P (2008).
13
14 47. Wang, J.-Q., Zhang, Z., Kuruppu, D. & Brownell, A.-L. Radiosynthesis of PET
15 radiotracer as a prodrug for imaging group II metabotropic glutamate receptors in
16 vivo. *Bioorg Med Chem Lett* **22**, 1958-1962 (2012).
17
18 48. Celen, S., Koole, M., Alcazar, J., De Angelis, M., Schmidt, M., Van Laere, K.,
19 Verbruggen, A., Langlois, X., Andres, J.I. & Bormans, G. Preliminary biological
20 evaluation of [¹¹C]JNJ42491293 as a radioligand for PET imaging of mGluR₂ in brain.
21 *J Nucl Med* **53**, 286 (2012).
22
23 49. Andrés, J.-I., Alcázar, J., Cid, J.M., De Angelis, M., Iturrino, L., Langlois, X.,
24 Lavreysen, H., Trabanco, A.A., Celen, S. & Bormans, G. Synthesis, Evaluation, and
25 Radiolabeling of New Potent Positive Allosteric Modulators of the Metabotropic
26 Glutamate Receptor 2 as Potential Tracers for Positron Emission Tomography
27 Imaging. *J Med Chem* **55**, 8685-8699 (2012).
28
29 50. Majo, V., Prabhakaran, J., Simpson, N., Arango, V., Mann, J.J. & Kumar, J.D.
30 Development of a [¹⁸F]-labeled positive allosteric modulator of the metabotropic
31 glutamate receptor 2 (mGluR₂) as a potential PET tracer. *J Nucl Med* **54**, 1072 (2013).
32
33 51. Ma, Y., Kumata, K., Yui, J., Zhang, Y., Yamasaki, T., Hatori, A., Fujinaga, M.,
34 Nengaki, N., Xie, L., Wang, H. & Zhang, M.-R. Synthesis and evaluation of
35 1-(cyclopropylmethyl)-4-(4-[¹¹C]methoxyphenyl)-piperidin-1-yl-2-oxo-1,2-dihydropy
36 ridine-3-carbonitrile ([¹¹C]CMDC) for PET imaging of metabotropic glutamate
37 receptor 2 in the rat brain. *Bioorg Med Chem* **25**, 1014-1021 (2017).
38
39 52. PCT/US2015/046962.
40 53. WO2016/087489A1.
41
42 54. Lavreysen, H., Langlois, X., Ahnaou, A., Drinkenburg, W., te Riele, P., Biesmans, I.,
43 Van der Linden, I., Peeters, L., Megens, A., Wintmolders, C., Cid, J.M., Trabanco,
44 A.A., Andres, J.I., Dautzenberg, F.M., Lutjens, R., Macdonald, G. & Atack, J.R.
45 Pharmacological characterization of JNJ-40068782, a new potent, selective, and
46 systemically active positive allosteric modulator of the mGlu2 receptor and its
47 radioligand [³H]JNJ-40068782. *J Pharmacol Exp Ther* **346**, 514-527 (2013).
48
49 55. Van Laere, K., Koole, M., de Hoon, J., Van Hecken, A., Langlois, X., Andres, J.I.,
50 Bormans, G. & Schmidt, M. Biodistribution, dosimetry and kinetic modeling of
51 [¹¹C]JNJ-42491293, a PET tracer for the mGluR₂ receptor in the human brain. *J Nucl*
52 *Med* **53**, 355 (2012).
53
54 56. Leurquin-Sterk, G., Celen, S., Van Laere, K., Koole, M., Bormans, G., Langlois, X.,
55 Van Hecken, A., te Riele, P., Alcázar, J., Verbruggen, A., de Hoon, J., Andrés, J.-I. &
56 Schmidt, M.E. What We Observe In Vivo Is Not Always What We See In Vitro:
57
58
59
60

- Development and Validation of ^{11}C -JNJ-42491293, A Novel Radioligand for mGluR₂. *J Nucl Med* **58**, 110-116 (2017).
57. McQuade, P., Joshi, A., Miller, P., Zeng, Z., Purcell, M., Gantert, L., Holahan, M., Meissner, R., Uslaner, J. & Hostetler, E. Discovery and Preclinical Evaluation of an mGluR₂-NAM PET Radioligand. *J Nucl Med* **57**, 290 (2016).
58. Lohith, T., McQuade, P., Salinas, C., Anderson, M., Reynders, T., Bautmans, A., Bormans, G., Serdons, K., Van Laere, K. & Hostetler, E. First-in-human PET imaging of mGluR₂ receptors. *J Nucl Med* **57**, 213 (2016).
59. WO2013/066736A1.
60. Niswender, C.M., Johnson, K.A., Luo, Q., Ayala, J.E., Kim, C., Conn, P.J. & Weaver, C.D. A novel assay of G_{i/o}-linked G protein-coupled receptor coupling to potassium channels provides new insights into the pharmacology of the group III metabotropic glutamate receptors. *Mol Pharmacol* **73**, 1213-1224 (2008).
61. Hemstapat, K., Da Costa, H., Nong, Y., Brady, A.E., Luo, Q., Niswender, C.M., Tamagnan, G.D. & Conn, P.J. A novel family of potent negative allosteric modulators of group II metabotropic glutamate receptors. *J Pharmacol Exp Ther* **322**, 254-264 (2007).
62. Kroeze, W.K., Sassano, M.F., Huang, X.P., Lansu, K., McCorvy, J.D., Giguere, P.M., Sciaky, N. & Roth, B.L. PRESTO-Tango as an open-source resource for interrogation of the druggable human GPCRome. *Nat Struct Mol Biol* **22**, 362-369 (2015).
63. Arunlakshana, O. & Schild, H.O. Some quantitative uses of drug antagonists. *Br J Pharmacol Chemother* **14**, 48-58 (1959).
64. Waterhouse, R.N. Determination of lipophilicity and its use as a predictor of blood-brain barrier penetration of molecular imaging agents. *Mol Imaging Biol* **5**, 376-389 (2003).
65. Patel, S. & Gibson, R. In vivo site-directed radiotracers: a mini-review. *Nucl Med Biol* **35**, 805-815 (2008).
66. Pike, V.W. Considerations in the Development of Reversibly Binding PET Radioligands for Brain Imaging. *Curr Med Chem* **23**, 1818-1869 (2016).
67. OECD. *Test No. 107: Partition Coefficient (n-octanol/water): Shake Flask Method*, (OECD Publishing).
68. Chung, T.D.Y., Terry, D.B. & Smith, L.H. *In Vitro and In Vivo Assessment of ADME and PK Properties During Lead Selection and Lead Optimization - Guidelines, Benchmarks and Rules of Thumb*, (Bethesda (MD): Eli Lilly & Company and the National Center for Advancing Translational Sciences; 2004-, 2015).
69. Gill, S.S. & Pulido, O.M. Glutamate receptors in peripheral tissues: current knowledge, future research, and implications for toxicology. *Toxicol Pathol* **29**, 208-223 (2001).
70. Andrés, J.-I., Alcázar, J., Cid, J.M., De Angelis, M., Iturrino, L., Langlois, X., Lavreysen, H., Trabanco, A.A., Celen, S. & Bormans, G. Synthesis, Evaluation, and Radiolabeling of New Potent Positive Allosteric Modulators of the Metabotropic Glutamate Receptor 2 as Potential Tracers for Positron Emission Tomography Imaging. *J Med Chem* **55**, 8685-8699 (2012).

71. Johnson, B.G., Wright, R.A., Arnold, M.B., Wheeler, W.J., Ornstein, P.L. & Schoepp, D.D. [³H]-LY341495 as a novel antagonist radioligand for group II metabotropic glutamate (mGlu) receptors: characterization of binding to membranes of mGlu receptor subtype expressing cells. *Neuropharmacology* **38**, 1519-1529 (1999).
72. Nikiforuk, A., Popik, P., Drescher, K.U., van Gaalen, M., Relo, A.L., Mezler, M., Marek, G., Schoemaker, H., Gross, G. & Besspalov, A. Effects of a positive allosteric modulator of group II metabotropic glutamate receptors, LY487379, on cognitive flexibility and impulsive-like responding in rats. *J Pharmacol Exp Ther* **335**, 665-673 (2010).
73. Harpoe, K., Isberg, V., Tehan, B.G., Weiss, D., Arsova, A., Marshall, F.H., Brauner-Osborne, H. & Gloriam, D.E. Selective Negative Allosteric Modulation Of Metabotropic Glutamate Receptors - A Structural Perspective of Ligands and Mutants. *Sci Rep* **5**, 13869 (2015).
74. Lundström, L., Bissantz, C., Beck, J., Wettstein, J.G., Woltering, T.J., Wichmann, J. & Gatti, S. Structural determinants of allosteric antagonism at metabotropic glutamate receptor 2: mechanistic studies with new potent negative allosteric modulators. *Br J Pharmacol* **164**, 521-537 (2011).
75. Rydberg, P., Gloriam, D.E., Zaretski, J., Breneman, C. & Olsen, L. SMARTCyp: A 2D Method for Prediction of Cytochrome P450-Mediated Drug Metabolism. *ACS Medicinal Chemistry Letters* **1**, 96-100 (2010).
76. Tatsuta, T., Naito, M., Oh-hara, T., Sugawara, I. & Tsuruo, T. Functional involvement of P-glycoprotein in blood-brain barrier. *J Biol Chem* **267**, 20383-20391 (1992).
77. Pike, V.W. PET Radiotracers: crossing the blood-brain barrier and surviving metabolism. *Trends Pharmacol Sci* **30**, 431-440 (2009).
78. Wang, L., Yui, J., Wang, Q., Zhang, Y., Mori, W., Shimoda, Y., Fujinaga, M., Kumata, K., Yamasaki, T., Hatori, A., Rotstein, B.H., Collier, T.L., Ran, C., Vasdev, N., Zhang, M.-R. & Liang, S.H. Synthesis and preliminary PET imaging studies of a FAAH radiotracer ([¹¹C]MPPPO) based on α -ketoheterocyclic scaffold. *ACS Chem Neurosci* **7**, 109-118 (2016).
79. Wang, L., Mori, W., Cheng, R., Yui, J., Hatori, A., Ma, L., Zhang, Y., Rotstein, B.H., Fujinaga, M., Shimoda, Y., Yamasaki, T., Xie, L., Nagai, Y., Minamimoto, T., Higuchi, M., Vasdev, N., Zhang, M.-R. & Liang, S.H. Synthesis and Preclinical Evaluation of Sulfonamido-based [¹¹C-Carbonyl]-Carbamates and Ureas for Imaging Monoacylglycerol Lipase. *Theranostics* **6**, 1145-1159 (2016).
80. Sidique, S., Dhanya, R.-P., Sheffler, D.J., Nickols, H.H., Yang, L., Dahl, R., Mangravita-Novo, A., Smith, L.H., D'Souza, M.S., Semenova, S., Conn, P.J., Markou, A. & Cosford, N.D.P. Orally Active Metabotropic Glutamate Subtype 2 Receptor Positive Allosteric Modulators: Structure-Activity Relationships and Assessment in a Rat Model of Nicotine Dependence. *J Med Chem* **55**, 9434-9445 (2012).
81. Dhanya, R.P., Sheffler, D.J., Dahl, R., Davis, M., Lee, P.S., Yang, L., Nickols, H.H., Cho, H.P., Smith, L.H., D'Souza, M.S., Conn, P.J., Der-Avakian, A., Markou, A. & Cosford, N.D. Design and synthesis of systemically active metabotropic glutamate subtype-2 and -3 (mGlu2/3) receptor positive allosteric modulators (PAMs):

- 1
2
3 pharmacological characterization and assessment in a rat model of cocaine
4 dependence. *J Med Chem* **57**, 4154-4172 (2014).
5
6 82. Wang, L., Mori, W., Cheng, R., Yui, J., Hatori, A., Ma, L., Zhang, Y., Rotstein, B.H.,
7 Fujinaga, M., Shimoda, Y., Yamasaki, T., Xie, L., Nagai, Y., Minamimoto, T.,
8 Higuchi, M., Vasdev, N., Zhang, M.-R. & Liang, S.H. Synthesis and Preclinical
9 Evaluation of Sulfonamido-based [¹¹C-Carbonyl]-Carbamates and Ureas for Imaging
10 Monoacylglycerol Lipase. *Theranostics* **6**, 1145-1159 (2016).
11
12 83. Reed, G.A. Stability of Drugs, Drug Candidates, and Metabolites in Blood and
13 Plasma. in *Curr Protoc Pharmacol*, Vol. 75 7.6.1-7.6.12 (John Wiley & Sons, Inc.,
14 2016).
15
16 84. Hill, J.R. In vitro drug metabolism using liver microsomes. in *Curr Protoc*
17 *Pharmacol*, Vol. 23 7.8:7.8.1-7.8.11 (2004).
18
19
20
21
22
23
24
25
26
27
28
29
30
31
32
33
34
35
36
37
38
39
40
41
42
43
44
45
46
47
48
49
50
51
52
53
54
55
56
57
58
59
60